Functionalization of graphene and Me-graphene: a molecular dynamics and DFT studies

Enesio Marinho Jr.[*] and Pedro A. S. Autreto[†]
Centro de Ciências Naturais e Humanas, Universidade Federal do ABC (UFABC),
Avenida dos Estados 5001, 09210-580 Santo André, São Paulo, Brazil

(Dated: December 11, 2020)

Graphene-based materials (GBMs) constitute a large family of materials which has attracted great interest for potential applications. In this work, we apply first-principles calculations based on density functional theory (DFT) and reactive molecular dynamics (MD) simulations to study the structural and electronic effects of hydrogenation in Me-graphene, a non-zero bandgap GBM composed of both sp^2 and sp^3-hybridized carbon. Our DFT results show a substantial tuning of the electronic properties of Me-graphene by hydrogenation, with the bandgap varying from 0.64 eV to 2.81 eV in the GGA-PBE approach, passing through metallic ground-states and a narrower bandgap state depending on the hydrogen coverage. The analyses of structural properties and binding energies have shown that hydrogenated Me-graphene presents strong and stable C−H bonds, and all of the carbon atoms are in sp^3 hybridization resulting in a boat-like favorable conformation for fully-hydrogenated Me-graphene. Our MD simulations have also indicated that the hydrogenation of Me-graphene is temperature-dependent, and the covalent adsorption tends to grow by islands.

I. INTRODUCTION

Graphene [1], a two-dimensional (2D) allotrope of carbon arranged on a honeycomb structure made out of hexagons [2], has shown exceptional physical, chemical and mechanical properties. It has a large theoretical specific surface area (2,630 $\mathrm{m^2\,g^{-1}}$) [3], high electron mobility at room temperature (250,000 $\mathrm{cm^2\,V^{-1}\,s^{-1}}$) [4], thermal conductivity in the order of 5000 $\mathrm{W\,mK^{-1}}$ [5], high Young's modulus (∼1.1 to 2.0 TPa) [6, 7], and good electrical conductivity [8, 9]. More recently, Cao *et al.* [10] experimentally demonstrated that bilayer graphene, which normally consists of two vertically stacked monolayer graphene layers arranged in an AB (Bernal) stacking configuration, when rotated at the so-called "magic angle" of ∼1.1° presents an intrinsic unconventional superconductivity for a critical temperature around 1.7 K.

Owing to this impressive gamma of astonishing properties, graphene has demonstrated outstanding performance in several applications such as catalysis [11], gas sensors [12], anti-corrosive coatings [13], flexible touchscreens [14], supercapacitors [15], transistors [16], spintronic [17], twistronics [18], energy storage [19], and most.

However, the synthesis of high-quality and large-area monolayer graphene in a cost effective process represents a drawback for industrial-scale applications [20]. In addition, the unmodified graphene has certain limitations, such as weak electrochemical activity, easy agglomeration and difficult processing, which greatly limit its applications [21]. Furthermore, this 2D nanomaterial is intrinsically a zero-gap semiconductor, or a semimetal, which turn it unsuitable for switching devices [22]. This are some of the reasons for the huge increase in the number of researches focused on functionalization of graphene including reactions with organic and inorganic molecules, chemical modification of the large graphene surface, and the general description of various covalent and non covalent interactions with it [23]. Chemical functionalization of graphene is a suitable approach to induce a tunable band gap opening [24], or to enable this material to be processed by solvent-assisted techniques, such as layer-by-layer assembly, spin-coating, and filtration [25].

The chemical functionalization by attaching hydrogen adatoms forming a fully hydrogenated graphene changes the hybridization of carbon atoms from sp^2 to sp^3, thus removing the conducting π-bands and opening a direct band gap at the Γ point with magnitude of 3.5-3.7 eV [26]. The so-called graphane is nonmagnetic semiconductor composed of 100% hydrogenated graphene, resulting in a CH stoichiometry. This graphene-based material was predicted to be stable in an extended covalently bonded 2D hydrocarbon with two favorable conformations: chair-like conformer, with the hydrogen atoms alternating on both sides of the plane and a boat-like conformer with the hydrogen adatoms alternating in pairs [26]. Graphane was first synthesized by Elias *et al.* using free-standing graphene, and further the authors have shown that reaction with hydrogen is reversible, so that the original metallic state, the lattice spacing, and even the quantum Hall effect can be restored by annealing [27].

Another important stable graphene derivative was already obtained using fluorine adatoms that strongly bind to carbons given rise to the so-called fluorographene, a 2D fully fluorinated graphene analogue of a fully fluorinated one-dimensional carbon chain known as Teflon. Fluorographene is a wide band gap semiconductor with $E_\mathrm{g} = 3.8$ eV, wide enough for optoelectronic applications in the blue/UV spectrum [28, 29].

Janus graphene (J-GN) has been predicted theoretically and prepared experimentally to study asymmetric chemistry of graphene functionalization [30–32]. The J-

---

[*] enesio.junior@ufabc.edu.br
[†] pedro.autreto@ufabc.edu.br

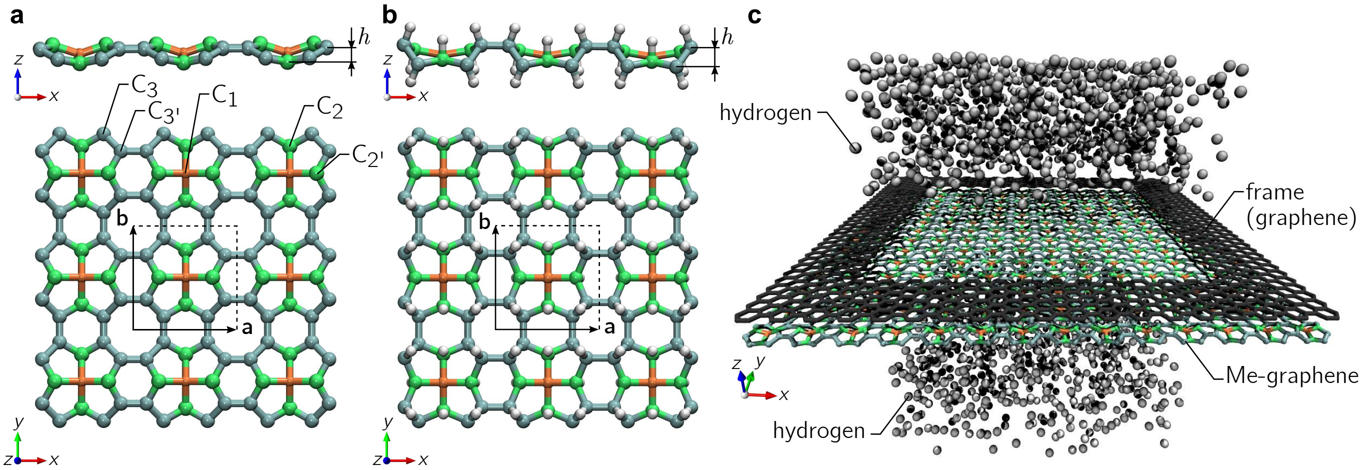

FIG. 1. Top and side view of optimized structure of (a) Me-graphene and (b) Me-graphane. We describe three types of carbon atoms, labeled as C_1 (sp^3) (orange), $C_2/C_{2'}$ (sp^2) (green) and $C_3/C_{3'}$ (sp^2) (blue). For Me-graphane, the hydrogen atoms are represented by white spheres. The buckling height is denoted by h. The unit cells are represented by doted square and lattice vectors **a** and **b**. (c) Representative structure used in the molecular dynamics simulations of the hydrogenation process of Me-graphene, in which we included a frame of graphene to prevent the bending or folding of the sheet.

GN is prepared achieving asymmetric covalent functionalization with a variety of functional groups on the opposite sides of graphene. The hydrofluorinated J-GN, namely fluorographone, is a semiconducting graphene derivative formed by covalent functionalization with hydrogen and fluorine adatoms being adsorbed onto the opposite sides of monolayer graphene [33]. Recently, we studied the modulation of hydrogen adsorption and the corresponding variation in electronic properties of hydrofluorinated J-GN [34].

The innovation arising out of graphene has boosted and inspired the research and development of novel 2D materials graphene-like allotropes such as graphyne's family [35], biphenylene carbon (BPC, also called graphenylene) [35–37], penta-graphene [38], pentahexoctite [39], T-graphene [40], octagraphene [41]. The carbon atoms in these allotropes are either sp^2 and/or sp hybridized. Interestingly, all these allotropes are planar and exhibit unique electronic as well as mechanical properties [39].

Zhuo *et al.* [42] have predicted a new dynamically stable 2D carbon allotrope named tertiary-methyl-graphene or Me-graphene (M-GN). This 2D carbon-based material is composed of both sp^2 and sp^3-hybridized carbon by topological assembly of $C-(C_3H_2)_4$ molecules. Consisting of a transitional ratio of sp^2 and sp^3-hybridized carbon atoms at the ratio of 12 : 1, M-GN is a transition between graphene (ratio 1 : 0) and penta-graphene (ratio 2 : 1). As expected, M-GN has transition properties between those of graphene and penta-graphene. For example, its band gap of 1.08 eV, which is between graphene (semimetal) and penta-graphene ($E_g = 3.25$ eV [38]). Furthermore, M-GN presents an unusual near zero Poisson's ratio of -0.002 up to 0.009 in the xy-plane, different from that of graphene (0.169) and penta-graphene (-0.068). M-GN also exhibits a high hole mobility of 1.60×10^5 $\mathrm{cm^2\,V^{-1}\,s^{-1}}$ at 300 K [42]. Those interesting properties of M-GN can be tuned by chemical functionalization, adsorbing for example hydrogen adatoms onto its surfaces. Indeed, this route tends to be explored in the future in order to open up new possibilities of applications for functionalized graphene-based materials.

Herein, we carried out a comprehensive atomistic study on the structural and electronic properties of M-GN covalent functionalized with hydrogen. For this purpose, we performed *ab initio* calculations based on density functional theory, as well as reactive molecular dynamics within the ReaxFF force field. We predicted dramatic changes in electronic and structural properties of M-GN by hydrogenation, and in its electronic and atomic structure, pushing forward the frontiers of novel semiconducting 2D materials based on covalent functionalization of graphene.

II. COMPUTATIONAL DETAILS

We performed *ab initio* calculations based on density functional theory [43, 44] as implemented in the Vienna ab initio simulation package (VASP) [45]. The projector augmented-wave method [46] was used to treat the electron-ion interaction, and the exchange-correlation functional was described by the generalized gradient approximation (GGA) as proposed by Perdew, Burke, and Ernzerhof (PBE) [47]. Structural optimizations were performed using a conjugate gradient algorithm until the residual forces on the atoms reach values smaller than 0.025 eV Å^{-1}. Kohn-Sham orbitals were expanded into a plane-wave basis set with kinetic energy up to 500 eV. The Brillouin zone was sampled using a Γ-centered 17×17×1 k-point mesh for the structural opti-

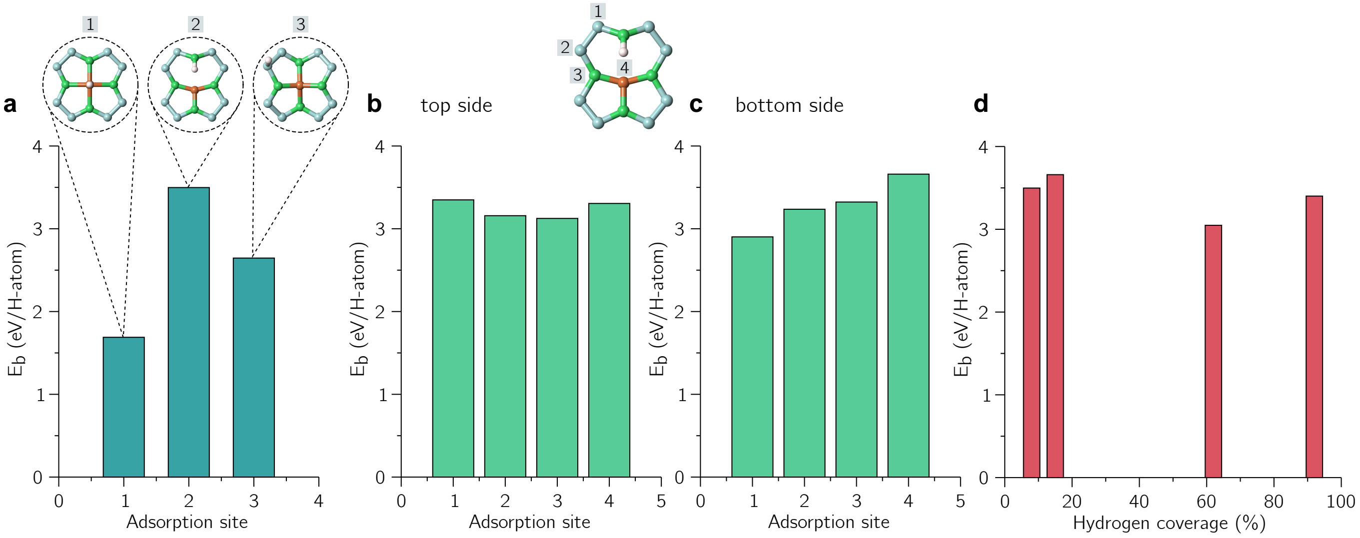

FIG. 2. Binding energies for hydrogenation of Me-graphene: (a) single-hydrogenated, double-hydrogenated on (b) top side and (c) bottom side, and (d) binding energies per hydrogen adatom as function of hydrogen coverage. The upper panels show the respective adsorption sites in Me-graphene structure.

TABLE I. Structural parameters for Me-graphene and Me-graphane.

		Me-graphene	Me-graphane
Lattice parameters (Å)	a	5.745	5.904
	b	5.745	5.905
	h	0.985	1.110
Bond lengths (Å)	C_1-C_2	1.563	1.614
	C_2-C_3	1.416	1.530
	$C_3-C_{3'}$	1.449	1.579
		1.406	1.549
Bond angles (°)	$C_1-C_2-C_3$	114.22	114.16
	$C_2-C_1-C_{2'}$	95.71	91.59

mization of Me-graphene, following the scheme proposed by Monkhorst and Pack [48]. Me-graphene monolayer and its images were separated by a vacuum space of ∼ 20 Å to avoid spurious interactions.

The crystal structure of M-GN is formed by twelve sp^2-hybridized and one sp^3-hybridized carbon atoms, as illustrated in Fig. 1(a), which can be described as methane with four hydrogen atoms replaced by cyclocopropenylidenes [42]. The ground-state structure posses a symmetry of $P\bar{4}m2$ (space group no. 115), containing carbon pentagons, hexagons, and octagons. The representative structure of fully-hydrogenated M-GN, named Me-graphane, is shown in Fig. 1(b). The modification of the sp^2-sp^2 carbon bonds by formation of sp^3-derived carbon-hydrogen bonds lead to the variation of structural conformation.

In addition, we carried out fully atomistic molecular dynamics (MD) simulations to study hydrogen adsorption and structural properties of hydrogenated Me-graphene at different temperatures. We employed the reactive force field (ReaxFF), which is is an empirical force field for reactive systems developed by van Duin *et al.* [49]. ReaxFF employs a bond order/bond energy relationship, which allows for bond formation and bond dissociation during molecular dynamics (MD) simulations. The bond orders are obtained from interatomic distances and are updated at every MD or energy minimization step [50]. ReaxFF MD simulations were implemented using the large-scale atomic/molecular massively parallel simulator (LAMMPS) code [51]. All ReaxFF MD simulations have been performed in the canonical (NVT) ensemble, with a time step of 0.25 fs using the Nosé-Hoover thermostat with a coupling time constant of 25 fs to control the temperature of the entire system. We modeled the hydrogenation employing a ∼ 80×80 Å M-GN supercell under a square 11Å wide frozen frame of monolayer graphene added to prevent bending or folding of the M-GN sheet during the MD, as shown in Fig. 1(c). We insert two hydrogen atmospheres into both top and bottom M-GN sides, confined to the exposed area of M-GN. Each hydrogen atmosphere is composed of 1,000 atoms in a volume of 58,300 Å^3.

III. RESULTS AND DISCUSSION

A. Structural properties of the pristine and hydrogenated Me-graphene

We analyze the structural modification of M-GN due to the incorporation of hydrogen adatoms on its surface. In Table I we present the optimzed lattice constants of M-GN, regarding a and b lattice vectors and buckling height

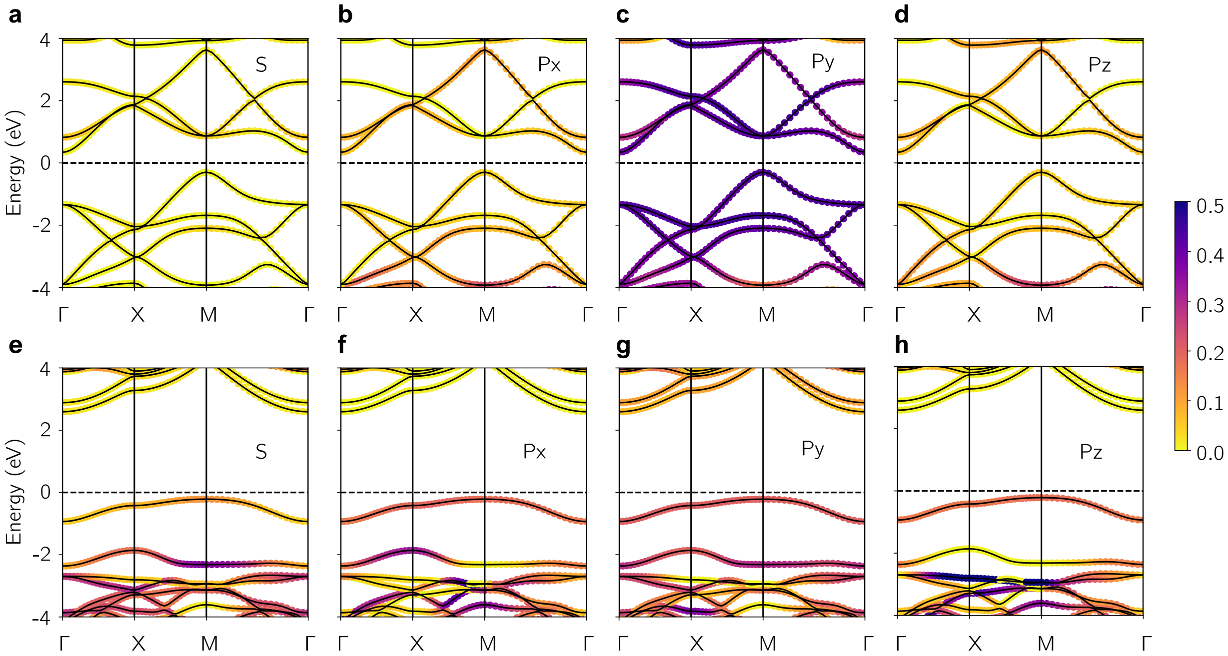

FIG. 3. Orbital-resolved bandstructures for the atomic orbitals (a) s, (b) p_x, (c) p_y and (d) p_z of Me-graphene, and for the orbitals (e) s, (f) p_x, (g) p_y and (h) p_z of Me-graphane. The Fermi level was set to zero on the energy axis.

h. We obtained $a = b = 5.745$ Å, with a thickness of $h = 0.985$ Å, in agreement with Ref. [42] ($a = b = 5.744$ Å and $h = 0.988$ Å). We analyzed three types of bond length between the sp^2-hybridized carbons, with values of 1.416, 1.449 and 1.406 Å, respectively, close to that of the C−C bond in graphene (1.426 Å). The bond length between sp^3-hybridized (C_1) and sp^2-hybridized (C_2) carbons was estimated in 1.563 Å. The bond angle among $C_1-C_2-C_3$ is 114.2 degrees, larger than the 109.47 degrees for standard sp^3 hybridization angle. The bond angle formed among $C_2-C_1-C_{2'}$ is 95.71 degrees.

Comparing the results of M-GN to those obtained for Me-graphane, we notice that the hydrogenation promotes an overall increase of the structural parameters, inducing a lattice strain of $\sim 2.8\%$. Every C−C bond lengths in Me-graphane are higher or similar to the sp^3 bond length of 1.548 Å in diamond and much greater than 1.426 Å characteristic of sp^2 C−C bond in graphene [26, 42]. We find that the boat-like conformer of Me-graphane is the most favorable conformation, with a buckling height of 1.110 Å. Similarly, the C−C bond lengths in graphane are 1.52 Å, much similar to that in diamond and shorter then C−C bond lengths in graphene. Furthermore, graphane has two favorable conformations, which are chair-like and boat-like conformers [26].

B. Hydrogen binding energy

We evaluate the most stable adsorption sites for hydrogenation calculating the hydrogen binding energies for different sites as the difference in total energy between the hydrogenated-compounds and their component parts as follows:

$$E_{\mathrm{b}} = -\left[\frac{E_{\text{M-GN}+n\mathrm{H}} - (E_{\text{M-GN}} + E_{+n\mathrm{H}})}{n}\right], \quad (1)$$

where $E_{\text{M-GN}+n\mathrm{H}}$ is the ground-state energy for the M-GN containing a total of n adsorbed hydrogen atoms, as well as $E_{\text{M-GN}}$ and $E_{n\mathrm{H}}$ are the energies for pristine M-GN and for an isolated hydrogen times the total number of hydrogen adsorbed, respectively. The results of binding energy per hydrogen in M-GN is shown in Fig. 2. The adsorption of one H into C_2 site of M-GN, corresponding to 7% of hydrogen coverage, leads to a 3.50 eV/H-atom binding energy (Fig. 2(a)). When H is adsorbed in C_2 site, the C_1-C_2 bond is broken, resulting in a decrease of the free energy due to a gain of conformational entropy yielding the highest binding energy.

We also analyze the hydrogen binding energy for a second adatom being inserted in single-hydrogenated M-GN, 8% of hydrogen coverage (Fig. 2(b)-(c)). Considering the H adsorption into the top side of M-GN, the highest binding energies were verified for the nearest-neighbor C_3 (index 1) and for the C_1 site, although the other two sites also present high binding energies above 3 eV/H-atom. For the H adsorption in the bottom side, the highest binding energy was achieved for the C_1 site. Finally, we study the binding energy for 62% of hydrogen coverage and for Me-graphane and, as a result, all the hydrogen binding energies were higher than 3 eV/H-atom. For comparison, the hydrogen binding energy in hydrogenated penta-graphene is 3.65 eV/H-atom [52], slightly higher than the ones obtained for hydrogenated M-GN.

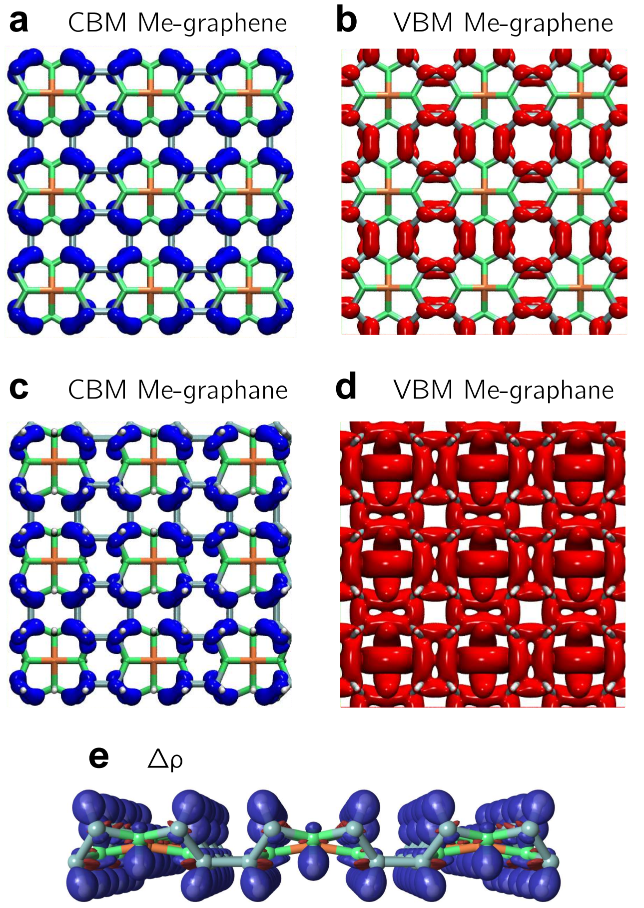

FIG. 4. Partial charge densities of VBM and CBM for (a-b) Me-graphene and (c-d) Me-graphane, with isosurfaces value 0.005 $e\,\text{Å}^{-3}$. (e) Charge density difference ($\Delta\rho$) plot for Me-graphane with isosurface value 0.015 $e\,\text{Å}^{-3}$. In $\Delta\rho$ results, blue and red regions depict charge accumulation and depletion, respectively.

TABLE II. Band gap and effective electron (m_e^*) and hole masses (m_h^*) in units of free electron mass m_0 at Γ and M points, respectively, using GGA-PBE approach.

H coverage (%)	E_g (eV)	m_e^*/m_0		m_h^*/m_0	
		Γ−X	Γ−M	M−X	M−Γ
0 (Me-graphene)	0.64	0.23	0.26	−0.21	−0.24
8	0	–	–	–	–
15	0.11	0.14	0.18	−0.27	−0.31
62	0	–	–	–	–
92 (Me-graphane)	2.81	1.02	1.02	−3.71	−3.37

Therefore, the hydrogenation of M-GN results in highly stable chemisorption and the resultant hydrogenated M-GN tends to be more energetically favorable due to the saturation of all nonplanar sp^2 hybridized carbon atoms.

C. Electronic structures

In Fig. 3, we show the orbital-resolved band structures for M-GN and Me-graphane. M-GN is an indirect band gap semiconductor with a band gap of 0.64 eV for GGA-PBE, which VBM at M point (0.5, 0.5, 0) and CBM at Γ point. This result is in excellent agreement with the reported theoretical band gap of 0.65 eV for M-GN [42] with identical band edges' coordinates. We also verify that the main contributions for VBM and CBM states around the Fermi level is from p_y orbitals, with small contributions from p_x and p_z. On the other hand, the electronic band structure of Me-graphene indicate that this is a wide band gap 2D semiconductor, presenting an indirect band gap with magnitude of 2.81 eV in GGA-PBE with band edges located also at M (VBM) and Γ (VBM). Near VBM, we notice the formation of a fully-filled intermediate band with bandwidth of about 1 eV. The main contribution for CBM in Me-graphane is from p_y orbitals as well, whereas VBM is formed by hybridization of p_x, p_y and p_z, with further a small contribution due to s orbitals from hydrogen atoms. Our results indicate that the intermediate band near VBM of Me-graphane occurs due to the conformation of hydrogenated M-GN, with main contributions of carbon-related orbitals and not directly by the presence of adsorbed hydrogen atoms. The partial charge density distributions for CBM and VBM of M-GN and Me-graphane are shown in Fig. 4(a)-(d). For M-GN, occupied-electron states of VBM and also empty CBM states are localized at octagonal rings, but with spatial separation. With regard to Me-graphane, CBM states lie in C_3-C_3 bonds of octagonal rings, whereas VBM states in Me-graphane are delocalized over all carbon bonds, in striking agreement with the orbital-resolved band structures.

In order to describe the effects of hydrogenation in the electron distribution of functionalized M-GN relative to the unperturbed system, we compute the charge density difference as follows

$$\Delta\rho = \rho_{\text{M-GN}+n\text{H}} - (\rho_{\text{M-GN}} + \rho_{n\text{H}}) \, , \tag{2}$$

where $\rho_{\text{M-GN}+n\text{H}}$ is the electron density of the hydrogenated M-GN containing a total of n hydrogen adatoms, and $\rho_{\text{M-GN}}$ and $\rho_{n\text{H}}$ are the unperturbed electron densities of the substrate and sorbate, respectively. The $\Delta\rho$ result is shown in Fig. 4(e). Our results indicate that p orbitals of carbon lost a small amount of electron density, verified through the depletion volumes in red. We also notive that the hydrogen adatoms effectively gained electrons, as we can see in the accumulation volumes in blue around hydrogen atoms, matching with the expectation to form C−H chemical bonds after adsorption.

Furthermore, to investigate the tuning of electronic properties of M-GN by hydrogenation, we calculate the electronic band gap and effective masses of charge carriers (electrons and holes) as a function of the amount of adsorbed hydrogen on its surface, and the results are described in Table II. The effective masses is a conve-

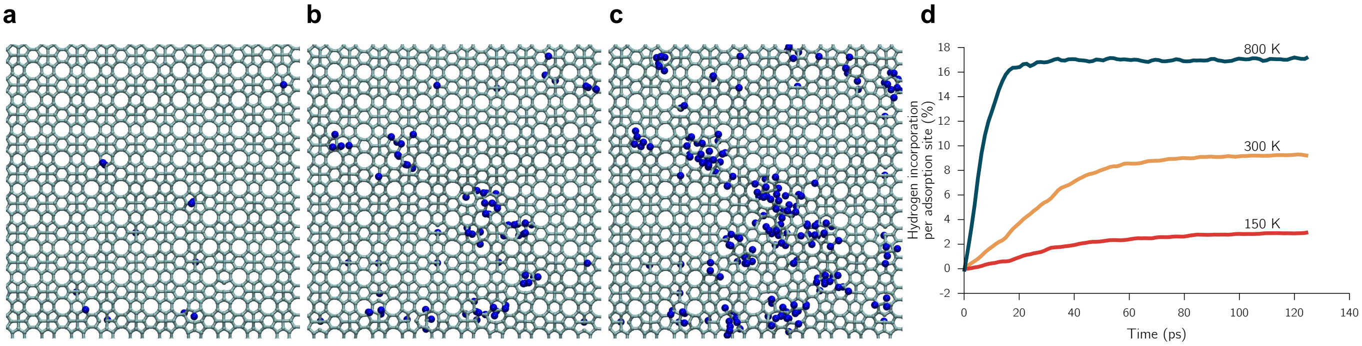

FIG. 5. Representative snapshots from the reactive molecular dynamics simulations of hydrogen incorporation process. H atoms are represented in blue. (a) Early stage, (b) intermediate stage, and (c) final stage of the adsorption dynamics. (d) Hydrogen rate incorporation per total adsorption site as a function of reaction time at 150, 300, and 800 K.

nient approach to obtain quantitative insights on the mobility of charge carriers. The effective electron (m_e^*) and holes (m_h^*) masses were derived from parabolic fits to the GGA-PBE band structures at the band extrema CBM and VBM, respectively, along the principal directions M$-$X and M$-\Gamma$ for VBM, and $\Gamma-$X and $\Gamma-$M for CBM. Our results indicate a dramatic variation of the band gap of M-GN by hidrogenation, ranging from 0.64 eV for pristine M-GN to 2.81 eV for Me-graphane. Moreover, for some intermediate concentrations of adsorbed hydrogen such as 8% and 62%, the hydrogenation produces metallic ground state of functionalized M-GN with band gap being vanished. On the other hand, for 15% of hydrogen coverage in M-GN we found a band gap of 0.11 eV which is substantially smaller than the band gap for pristine M-GN. This hydrogenated M-GN system was modeled adsorbing one H on C_2-site (top side) and the other H adsorbed onto nearest-neighbor C_3-site.

The effective masses are also effectively tailored with changes in hydrogen coverage of M-GN. The effective electron and hole masses in pristine M-GN are similar, with $m_e^* = 0.23\, m_0$ (in $\Gamma-$X direction) and $m_h^* = 0.21\, m_0$ (in M$-$X direction). Comparing to penta-graphene which presents $m_e^* = 0.24\, m_0$ and $m_h^* = 0.50\, m_0$ in GGA-PBE [53], the effective hole mass in M-GN tends to be lower while the effective electron mass is similar. Our results for Me-graphane show that the effective masses significantly increase. We compute $m_e^* = 1.02\, m_0$ and $m_h^* = 3.71\, m_0$ in GGA-PBE for Me-graphene. Similarly, the effective masses for hydrogenated penta-graphene, named penta-graphane, also tends to be higher than those in pristine penta-graphene, with $m_e^* = 1.2\, m_0$ and $m_h^* = 0.58\, m_0$ in GGA-RPBE approach [54]. In addition, the effective masses in 15%-hydrogenated M-GN vary to a lower value for electrons, with $m_e^* = 0.14\, m_0$ in $\Gamma-$X, and keeping in the same order of magnitude for holes, with $m_h^* = 0.27\, m_0$ in M$-$X direction.

The hydrogen adsorption dynamics was analyzed by reactive MD simulations. In Fig. 5(a)-(c) we present representative snapshots from a 0.12 ns MD simulation of the hydrogenation process in M-GN at 300 K for a atmosphere composed only of F atoms. At ealier stage, Fig. 5(a), we notice that the H atoms are mostly incorporated on C_2-sites, acting as seeds to the growth of hydrogen islands in the next stages of hydrogenation. In Fig. 5(d) we show the curves of hydrogenation per total adsorption sites as a function of reaction time. We considered the hydrogen adsoption at temperatures of 150, 300, and 800 K. As a result, the hydrogen rate incorporation can be represented in two phases, at the beginning by linear upward curve followed by a plato indicating the saturation of adsorption and therefore reaching the dynamic equilibrium. Since the saturation is achieved for different reaction times regarding the increase in temperature, this suggest that the hydrogenation of M-GN is temperature-dependent, similar to the atomistic results of functionalization of graphene reported in literature. Our reactive MD simulations also show that the C_1-C_2 bond tends to be broken due to vibrational effects, favoring the formation of defects and turning the C_1 site into a more favorable adsorption site.

IV. SUMMARY AND CONCLUSIONS

Motivated by the promising properties of a new graphene-based semiconductor named Me-graphene, we have studied the effects of hydrogenation on structural and electronic properties of this 2D nanomaterial. Our *ab initio* DFT calculations show a dramatic tuning of the electronic properties of M-GN by hydrogenation. M-GN is a semicondutor with indirect band gap of 0.64 eV, whereas fully-hydrogenated M-GN (named Me-graphane) is a wide band gap semiconductor with $E_\mathrm{g} = 2.81$ eV in GGA-PBE approach. Analyzing intermediate hydrogen concentrations for partial functionalization of M-GN we found metallic ground-states a semiconducting state for 15%-hydrogenated M-GN, with narrow band gap of 0.11 eV. The insertion of hydrogen adatoms up to Me-graphane tends to increase both the effective electron and hole masses, although for 15%-hydrogenated M-GN the effective electron mass decrease and the effective hole mass is maintained is held at the same order of magnitude. The hydrogen atoms bind strongly to M-GN during functionalization, with binding energies higher than 3 eV. Me-graphane presents higher bond lenghts compared to M-GN ones, and its most favorable conformation is boat-like. The reactive molecular dynamics simulation shows that the hydrogenation of M-GN is a temperature-dependent reaction, with formation of hydrogen islands starting with adsorptions in the most stable carbon site. In summary, if the synthesis of M-GN and Me-graphane is carried out, those graphene-based low-dimensional semiconductors will boost the range of potential applications of carbon-allotropes.

ACKNOWLEDGMENTS

This work was supported by the Brazilian agencies FAPESP and CAPES. Computational resources were provided by the high performance computing center at UFABC. The authors thank Mr. Matheus Medina for his technical support in reactive molecular dynamics simulations.

[1] K. S. Novoselov, A. K. Geim, S. V. Morozov, D. Jiang, Y. Zhang, S. V. Dubonos, I. V. Grigorieva, and A. A. Firsov, Electric field effect in atomically thin carbon films, Science **306**, 666 (2004).

[2] A. H. Castro Neto, F. Guinea, N. M. R. Peres, K. S. Novoselov, and A. K. Geim, The electronic properties of graphene, Rev. Mod. Phys. **81**, 109 (2009).

[3] Y. Zhu, S. Murali, W. Cai, X. Li, J. W. Suk, J. R. Potts, and R. S. Ruoff, Graphene and graphene oxide: synthesis, properties, and applications, Adv. Mater. **22**, 3906 (2010).

[4] K. S. Novoselov, A. K. Geim, S. V. Morozov, D. Jiang, M. I. Katsnelson, I. V. Grigorieva, S. V. Dubonos, and A. A. Firsov, Two-dimensional gas of massless dirac fermions in graphene, Nature **438**, 197 (2005).

[5] A. A. Balandin, S. Ghosh, W. Bao, I. Calizo, D. Teweldebrhan, F. Miao, and C. N. Lau, Superior thermal conductivity of single-layer graphene, Nano Lett. **8**, 902 (2008).

[6] C. Lee, X. Wei, J. W. Kysar, and J. Hone, Measurement of the elastic properties and intrinsic strength of monolayer graphene, Science **321**, 385 (2008).

[7] J.-W. Jiang, J.-S. Wang, and B. Li, Young's modulus of graphene: A molecular dynamics study, Phys. Rev. B **80**, 113405 (2009).

[8] D. G. Papageorgiou, I. A. Kinloch, and R. J. Young, Mechanical properties of graphene and graphene-based nanocomposites, Prog. Mater. Sci. **90**, 75 (2017).

[9] P. Głuchowski, R. Tomala, A. Jeżowski, D. Szewczyk, B. Macalik, I. Smolina, T. Kurzynowski, and W. Stręk, Preparation and physical characteristics of graphene ceramics, Sci. Rep. **10**, 1 (2020).

[10] Y. Cao, V. Fatemi, S. Fang, K. Watanabe, T. Taniguchi, E. Kaxiras, and P. Jarillo-Herrero, Unconventional superconductivity in magic-angle graphene superlattices, Nature **556**, 43 (2018).

[11] B. F. Machado and P. Serp, Graphene-based materials for catalysis, Catal. Sci. Technol. **2**, 54 (2012).

[12] W. Yuan and G. Shi, Graphene-based gas sensors, J. Mater. Chem. A **1**, 10078 (2013).

[13] G. Cui, Z. Bi, R. Zhang, J. Liu, X. Yu, and Z. Li, A comprehensive review on graphene-based anti-corrosive coatings, Chem. Eng. J. **373**, 104 (2019).

[14] A. Vlasov, D. Terent'ev, and V. Shakhnov, Graphene flexible touchscreen with integrated analog-digital converter, Russ. Microelectron. **46**, 192 (2017).

[15] Y. Wang, Z. Shi, Y. Huang, Y. Ma, C. Wang, M. Chen, and Y. Chen, Supercapacitor devices based on graphene materials, J. Phys. Chem. C **113**, 13103 (2009).

[16] F. Schwierz, Graphene transistors, Nat. Nanotechnol. **5**, 487 (2010).

[17] W. Han, R. K. Kawakami, M. Gmitra, and J. Fabian, Graphene spintronics, Nat. Nanotechnol. **9**, 794 (2014).

[18] S. Carr, D. Massatt, S. Fang, P. Cazeaux, M. Luskin, and E. Kaxiras, Twistronics: Manipulating the electronic properties of two-dimensional layered structures through their twist angle, Phys. Rev. B **95**, 075420 (2017).

[19] A. Olabi, M. A. Abdelkareem, T. Wilberforce, and E. T. Sayed, Application of graphene in energy storage device–a review, Renew. Sust. Energ. Rev. **135**, 110026 (2021).

[20] L. Lin, H. Peng, and Z. Liu, Synthesis challenges for graphene industry, Nat. Mater. **18**, 520 (2019).

[21] W. Yu, L. Sisi, Y. Haiyan, and L. Jie, Progress in the functional modification of graphene/graphene oxide: a review, RSC Adv. **10**, 15328 (2020).

[22] F. Pulizzi, O. Bubnova, S. Milana, D. Schilter, D. Abergel, and A. Moscatelli, Graphene in the making, Nat. Nanotechnol. **14**, 914 (2019).

[23] V. Georgakilas, M. Otyepka, A. B. Bourlinos, V. Chandra, N. Kim, K. C. Kemp, P. Hobza, R. Zboril, and K. S. Kim, Functionalization of graphene: covalent and non-covalent approaches, derivatives and applications, Chem. Rev. **112**, 6156 (2012).

[24] M. Pumera, Heteroatom modified graphenes: electronic and electrochemical applications, J. Mater. Chem. C **2**, 6454 (2014).

[25] T. Kuila, S. Bose, A. K. Mishra, P. Khanra, N. H. Kim, and J. H. Lee, Chemical functionalization of graphene and its applications, Prog. Mater. Sci. **57**, 1061 (2012).

[26] J. O. Sofo, A. S. Chaudhari, and G. D. Barber, Graphane: A two-dimensional hydrocarbon, Phys. Rev. B **75**, 153401 (2007).

[27] D. C. Elias, R. R. Nair, T. Mohiuddin, S. Morozov, P. Blake, M. Halsall, A. C. Ferrari, D. Boukhvalov, M. Katsnelson, A. Geim, *et al.*, Control of graphene's properties by reversible hydrogenation: evidence for graphane, Science **323**, 610 (2009).

[28] R. R. Nair, W. Ren, R. Jalil, I. Riaz, V. G. Kravets, L. Britnell, P. Blake, F. Schedin, A. S. Mayorov, S. Yuan, *et al.*, Fluorographene: a two-dimensional counterpart of teflon, Small **6**, 2877 (2010).

[29] K.-J. Jeon, Z. Lee, E. Pollak, L. Moreschini, A. Bostwick, C.-M. Park, R. Mendelsberg, V. Radmilovic, R. Kostecki, T. J. Richardson, *et al.*, Fluorographene: a wide bandgap semiconductor with ultraviolet luminescence, Acs Nano **5**, 1042 (2011).

[30] M. Yang, R. Zhao, J. Wang, L. Zhang, Q. Xie, Z. Liu, and Z. Liu, Bandgap opening in janus-type mosaic graphene, J. Appl. Phys. **113**, 084313 (2013).

[31] F. Li and Y. Li, Band gap modulation of janus graphene nanosheets by interlayer hydrogen bonding and the external electric field: a computational study, J. Mater. Chem. C **3**, 3416 (2015).

[32] L. Zhang, J. Yu, M. Yang, Q. Xie, H. Peng, and Z. Liu, Janus graphene from asymmetric two-dimensional chemistry, Nat. Commun. **4**, 1 (2013).

[33] Y. Jin, Q. Xue, L. Zhu, X. Li, X. Pan, J. Zhang, W. Xing, T. Wu, and Z. Liu, Self-assembly of hydrofluorinated janus graphene monolayer: a versatile route for designing novel janus nanoscrolls, Sci. Rep. **6**, 26914 (2016).

[34] G. R. Schleder, E. Marinho Jr., D. J. R. Baquiao, Y. M. Celaschi, F. Gollino, G. M. Dalpian, and P. A. S. Autreto, Tuning hydrogen adsorption and electronic properties from graphene to fluorographone, Phys. Rev. Mater. **4**, 074005 (2020).

[35] R. Baughman, H. Eckhardt, and M. Kertesz, Structure-property predictions for new planar forms of carbon: Layered phases containing sp^2 and sp atoms, J. Chem. Phys. **87**, 6687 (1987).

[36] G. Brunetto, P. Autreto, L. Machado, B. Santos, R. P. Dos Santos, and D. S. Galvao, Nonzero gap two-dimensional carbon allotrope from porous graphene, J. Phys. Chem. C **116**, 12810 (2012).

[37] A. N. Enyashin and A. L. Ivanovskii, Graphene allotropes, physica status solidi (b) **248**, 1879 (2011).

[38] S. Zhang, J. Zhou, Q. Wang, X. Chen, Y. Kawazoe, and P. Jena, Penta-graphene: A new carbon allotrope, PNAS **112**, 2372 (2015).

[39] B. R. Sharma, A. Manjanath, and A. K. Singh, pentahexoctite: A new two-dimensional allotrope of carbon, Sci. Rep. **4**, 1 (2014).

[40] Y. Liu, G. Wang, Q. Huang, L. Guo, and X. Chen, Structural and electronic properties of T graphene: a two-dimensional carbon allotrope with tetrarings, Phys. Rev. Lett. **108**, 225505 (2012).

[41] X.-L. Sheng, H.-J. Cui, F. Ye, Q.-B. Yan, Q.-R. Zheng, and G. Su, Octagraphene as a versatile carbon atomic sheet for novel nanotubes, unconventional fullerenes, and hydrogen storage, J. Appl. Phys. **112**, 074315 (2012).

[42] Z. Zhuo, X. Wu, and J. Yang, Me-graphene: a graphene allotrope with near zero poisson's ratio, sizeable band gap, and high carrier mobility, Nanoscale **12**, 19359 (2020).

[43] P. Hohenberg and W. Kohn, Inhomogeneous electron gas, Phys. Rev. **136**, B864 (1964).

[44] W. Kohn and L. J. Sham, Self-consistent equations including exchange and correlation effects, Phys. Rev. **140**, A1133 (1965).

[45] G. Kresse and J. Furthmüller, Efficient iterative schemes for ab initio total-energy calculations using a plane-wave basis set, Phys. Rev. B **54**, 11169 (1996).

[46] P. E. Blöchl, Projector augmented-wave method, Phys. Rev. B **50**, 17953 (1994).

[47] J. P. Perdew, K. Burke, and M. Ernzerhof, Generalized gradient approximation made simple, Phys. Rev. Lett. **77**, 3865 (1996).

[48] H. J. Monkhorst and J. D. Pack, Special points for brillouin-zone integrations, Phys. Rev. B **13**, 5188 (1976).

[49] A. C. T. van Duin, S. Dasgupta, F. Lorant, and W. A. Goddard, Reaxff: a reactive force field for hydrocarbons, J. Phys. Chem. A **105**, 9396 (2001).

[50] M. Raju, S.-Y. Kim, A. C. Van Duin, and K. A. Fichthorn, Reaxff reactive force field study of the dissociation of water on titania surfaces, J. Phys. Chem. C **117**, 10558 (2013).

[51] S. Plimpton, Fast parallel algorithms for short-range molecular dynamics, J. Comput. Phys. **117**, 1 (1995).

[52] X. Li, S. Zhang, F. Q. Wang, Y. Guo, J. Liu, and Q. Wang, Tuning the electronic and mechanical properties of penta-graphene via hydrogenation and fluorination, Phys. Chem. Chem. Phys. **18**, 14191 (2016).

[53] J. Deb, N. Seriani, and U. Sarkar, Ultrahigh carrier mobility of penta-graphene: A first-principle study, Phys. E Low Dimens. Syst. Nanostruct. , 114507 (2020).

[54] H. Einollahzadeh, S. M. Fazeli, and R. S. Dariani, Studying the electronic and phononic structure of pentagraphane, Sci. Technol. Adv. Mater. **17**, 610 (2016).